Myocardial Imaging: Tissue Doppler and Speckle Tracking

EDITED BY

Thomas H. Marwick, MBBS, PhD

Professor of Medicine, University of Queensland
Princess Alexandra Hospital
Brisbane, Australia

Cheuk-Man Yu, MBChB

Head, Division of Cardiology
Department of Medicine and Therapeutics
The Chinese University of Hong Kong
Prince of Wales Hospital, Shatin, N.T.
Hong Kong

Jing Ping Sun, MD

Associate Professor of Medicine
The Carlyle Fraser Heart Center
Cardiology Department
Atlanta, GA
USA

Blackwell
Publishing

Myocardial Imaging: Tissue Doppler and Speckle Tracking

To my three Muses – Rosey, Victoria and Tess

Thomas H. Marwick

My respected parents, Tit-ngan and Chan-siu Yu,
My beloved wife, Joan,
My dear sons, Yannick and Ryan,
for their love and support

C.M. Yu

To my husband, Dr. Xing Sheng Yang,
for continued support of my efforts

Jing-Ping Sun

Myocardial Imaging: Tissue Doppler and Speckle Tracking

EDITED BY

Thomas H. Marwick, MBBS, PhD

Professor of Medicine, University of Queensland
Princess Alexandra Hospital
Brisbane, Australia

Cheuk-Man Yu, MBChB

Head, Division of Cardiology
Department of Medicine and Therapeutics
The Chinese University of Hong Kong
Prince of Wales Hospital, Shatin, N.T.
Hong Kong

Jing Ping Sun, MD

Associate Professor of Medicine
The Carlyle Fraser Heart Center
Cardiology Department
Atlanta, GA
USA

Blackwell
Publishing

Blackwell Futura is an imprint of Blackwell Publishing

Blackwell Publishing, Inc., 350 Main Street, Malden, Massachusetts 02148-5020, USA
Blackwell Publishing Ltd, 9600 Garsington Road, Oxford OX4 2DQ, UK
Blackwell Science Asia Pty Ltd, 550 Swanston Street, Carlton, Victoria 3053, Australia

First published 2007

1 2007

ISBN: 978-1-4051-6113-8

Library of Congress Cataloging-In-Publication/Data

Myocardial imaging / edited by Thomas H. Marwick, Cheuk-Man Yu, Jing Ping Sun.
p. ; cm.
Includes bibliographical references and index.
ISBN 978-1-4051-6113-8 (alk. paper)
1. Echocardiography. 2. Myocardium — Ultrasonic imaging. I. Marwick, Thomas H. II. Yu, Cheuk-Man. III. Sun, Jingping.
[DNLM: 1. Heart — radionuclide imaging. 2. Angiocardiography. WG 141.5.R2 M9966 2007]
RC683.5.U5M97 2007
616.1'207543 — dc22

2007000374

A catalogue record for this title is available from the British Library

Commissioning Editor: Gina Almond
Development Editor: Fiona Pattison
Editorial Assistant: Victoria Pitman
CD produced by: Meg Barton and Nathan Harris

Set in 9.5/12pt Minion by Newgen Imaging Systems (P) Ltd, Chennai, India
Printed and bound in Singapore by Fabulous Printers Pte Ltd

For further information on Blackwell Publishing, visit our website:
www.blackwellcardiology.com

Contents

A companion CD-ROM with 32 videoclips and a figure database is included at the back of the book

Contributors

Svein A. Aase
Master of Science in Computer Science
Medinsk Teknisk Forskningssenter
NO-7489
Norway

Theodore P. Abraham, MD, FACC, FASE
Johns Hopkins University
Baltimore, MD, USA

Niels Holmark Andersen, PhD
Medical Department M (Diabetes & Endocrinology)
Aarhus University Hospital
Nørrebrogade 44
DK-8000 Aarhus C
Denmark

Craig R. Asher, MD, FACC
The Department of Cardiovascular Imaging
The Cleveland Clinic Foundation
Cleveland, Ohio, USA

Jeroen J. Bax, MD
Department of Cardiology
Leiden University Medical Center
Leiden
The Netherlands

Patrick E. BeDell, BBA, RDCS, FASE
Technical Director/Core Lab Manager
The Emory Clinic
Crawford Long Hospital, USA

Charlotte Bjork-Ingul, MD
Department of Cardiology
Norwegian Technical University
Trondheim
Norway

Gabe B. Bleeker, MD
Department of Cardiology
Leiden University Medical Center
Leiden
The Netherlands

Jan D'hooge, PhD
Medical Image Computing
Department of Cardiology
Catholic University Leuven
Leuven
Belgium

Geneviève Derumeaux
Department of Cardiology
CHU de Lyon
Hôpital Cardio-vasculaire et Pneumologique
Louis PRADEL
28 Avenue Doyen Lépine
69500 Bron
France

Vitantonio Di Bello
Associate Professor of Cardiology
Cardiac Ultrasound Laboratory
Cardiac and Thoracic Department
University of Pisa
Italy

Thor Edvardsen, MD, PhD
Director of Cardiovascular Imaging Research
Department of Cardiology
Rikshospitalet University Hospital
University of Oslo, Oslo
Norway

Neil L. Greenberg, PhD
The Department of Cardiovascular Imaging
The Cleveland Clinic Foundation
Cleveland, Ohio, USA

Jeffrey Wing-Hong Fung MBChB, MRCP, FHKCP, FHKAM, FRCP
Director of Pacing and Electrophysiology Services
Division of Cardiology
Department of Medicine and Therapeutics
Prince of Wales Hospital
The Chinese University of Hong Kong
Hong Kong

Jong-Won Ha, MD, PhD
Associate Professor
Cardiology Division
Yonsei University College of Medicine
Seoul
South Korea

Brian A. Haluska, MSc, RDCS, AMS, FASE
UQ Department of Medicine
Princess Alexandra Hospital
Brisbane, Q4102
Australia

Andreas Heimdal, MSc, PhD
Research and Development Engineer
GE Vingmed Ultrasound
Forskningsparken
Gaustadalléen 21
0349 Oslo
Norway

Rainer Hoffmann, MD, FESC
Senior Staff Cardiologist
Medical Clinic I
University Aachen
Lamwelsstrasse
52097 Aachen
Germany

Eduard R. Holman
Department of Cardiology
Leiden University Medical Center
Leiden
The Netherlands

Hsin-Yueh Liang
Johns Hopkins University
Baltimore, MD, USA

Sunil V. Mankad, MD, FACC, FASE
Assistant Professor, Internal Medicine and Cardiovascular Disease
Senior Associate Consultant, Cardiovascular Diseases
Echocardiography Laboratory
Mayo Clinic College of Medicine
Rochester, MN, USA

Thomas H. Marwick, MBBS, PhD
Professor of Medicine, University of Queensland,
Princess Alexandra Hospital, Brisbane,
Q4102, Australia

John D. Merlino, MD, FACC
Division of Cardiology
Emory Crawford Long Campus
Atlanta, GA, USA

Sherif F. Nagueh, MD, FACC
Professor of Medicine, Weill Medical College
Cornell University
6550 Fannin SM-677
The Methodist Hospital
Houston, TX 77030-2717
United States

Jae K. Oh, MD, FACC, FAHA
Professor, Internal Medicine and Cardiovascular Disease
Co-director, Echocardiography Laboratory
Director, Echocardiography Core Lab
Consultant, Cardiovascular Diseases
Mayo Clinic College of Medicine
Rochester, MN, USA

Seong-Mi Park, MD, PhD
Assistant Professor, Internal Medicine and Cardiology
Cardiovascular Center, Anam Hospital
College of medicine, Korea University
Seoul, Korea

Zoran B. Popović, MD
The Department of Cardiovascular Imaging
The Cleveland Clinic Foundation
Cleveland, Ohio, USA

John E. Sanderson, MA, MD, FRCP, FACC
Professor of Cardiology & Consultant Cardiologist
Keele University Medical School, University Hospotal of
North Staffordshire; Department of Cardiology,
City General Hospital, Stoke On Trent, UK

James E. Sharman, PhD
Department of Medicine
University of Queensland
Princess Alexandra Hospital
Brisbane, Australia

Otto A. Smiseth, MD, PhD
Department of Cardiology
Rikshospitalet University Hospital
University of Oslo, Norway

William J. Steward, MD, FACC
The Department of Cardiovascular Imaging
The Cleveland Clinic Foundation
Cleveland, Ohio, USA

Asbjorn Stoylen, MD
Associate Professor
Department of Circulation and Medical Imaging
Faculty of Medicine
Norwgian University of Science and Technology
Medisinsk teknisk forskningssenter
N-7489 Trondheim
Norway

Joerg M. Strotmann, MD
Department of Internal Medicine I/Center of Cardiovascular Disease
University of Wuerzburg
Germany

Jing Ping Sun, MD, FACC, FAHA
Associate Professor of Medicine
The Carlyle Fraser Heart Center
Cardiology Department, 6th Floor
Atlanta, Georgia
USA

James D. Thomas, MD, FACC
The Department of Cardiovascular Imaging
The Cleveland Clinic Foundation
Cleveland, Ohio, USA

Sudhir Wahi, MD, FRCP, FCSANZ
Department of Cardiology
Princess Alexandra Hospital
Ipswitch Road, Brisbane
Queensland
Australia

Jianwen Wang, PhD, MD
The Echocardiography laboratory of the Methodist DeBakey Heart Center
The Methodist Hospital, Houston
Texas, USA

Frank Weidemann, MD
Department of Internal Medicine I/Center of Cardiovascular Disease
University of Wuerzburg
Germany

Gabriel W. Yip, MD, MRCP, FACC, FASE
Department of Medicine and Therapeutics
Prince of Wales Hospital
Shatin, NT
Hong Kong
China

Cheuk-Man Yu MBChB, MRCP, MD, FHKCP, FHKAM, FRACP, FRCP
Professor
Head of Division of Cardiology
Department of Medicine and Therapeutics
Prince of Wales Hospital
The Chinese University of Hong Kong
Hong Kong

Qing Zhang, BM, MM, PhD
Research Assistant Professor
Division of Cardiology
Department of Medicine and Therapeutics
Prince of Wales Hospital
The Chinese University of Hong Kong
Hong Kong

Xiao-Fang Xu, MD, PhD
The Department of Cardiovascular Imaging
The Cleveland Clinic Foundation
Cleveland, Ohio, USA

Foreword

It has been barely 50 years since Inge Edler and Helmut Hertz first used an ultrasound transducer—purloined from a Malmo shipyard where it was used to examine the hulls of ships—to record the motion of structures in their hearts, not knowing whether the ultrasonic energy might rupture their ventricles. In the relatively brief interim, we have seen staggering technical progress: A-mode, M-mode, B-mode, PW, CW, color Doppler, TEE, digital echo, stress echo, contrast perfusion, tissue harmonics, 3D, and on and on. Over the past 10 years, however, perhaps the most important advance has been the development of techniques to quantify tissue motion and deformation. These techniques—tissue Doppler and speckle tracking imaging—have fundamentally altered the way echocardiography approaches the characterization of global and regional myocardial function. The notion that tissue motion—as opposed to endocardial excursion—is useful in the assessment of ventricular function is hardly new: Derek Gibson utilized M-mode over 30 years ago to relate myocardial velocity to ventricular function. What these new methods provide is an unprecedented view of tissue motion on a region-by-region basis. Exploiting the revolution in image quality, parallel processing, and digital storage and analysis that has also occurred in this time period, giving us 2D and color Doppler frame rates exceeding 100 Hz, these methods have literally launched a thousand (at least) research papers describing applications in ventricular physiology, heart failure management, ischemia and viability assessment, ventricular synchrony, and valvular heart disease.

What has been lacking in much of this work has been practical instruction in how to apply these new methods in routine clinical practice. So many times I have been addressing audiences of advanced echocardiographers in the United States and abroad only to find that TDI and speckle tracking, while unquestioned in their utility, are rarely used in routine clinical assessment. This is the gap that I believe this book will help fill. Drawing on the expertise of many of the individuals who developed and validated these techniques in the first place, these chapters describe not just the technical background and research validation of these methods but also provide practical outlines of how to integrate them into routine clinical practice in a busy echo lab. All the brilliant research in the world is of little value if a new technique is rarely used.

On a personal level, I am especially pleased to see this book coming from these particular editors. Not only has CM Yu combined his renaissance-man skills in heart failure management, electrophysiology, and echocardiography to define the tissue Doppler criteria for LV synchrony, but he is also a dear friend with whom I fondly remember sharing oysters at the top of the Hong Kong Sheraton among many other good times. Jing Ping Sun worked with me at the Cleveland Clinic for over a decade, validating the clinical utility of many of the new technologies to emerge during this period. Calling herself my "Chinese mother" she has taught me much about the role of dedication and perseverance in succeeding, which in her case included overcoming two years of "reeducation" during the Cultural Revolution in China, completely separated from her family and work. I've likened her tenacity on any project to a "pit-bull on a porkchop", and I have no doubt that this book reflects this same determination. Finally, Tom Marwick is simply one of the most focused and organized researchers in the world, investigating the role of new imaging

technologies in real-world problems like ischemia, viability, cardiomyopathies, and the impact of systemic diseases like diabetes on the heart. Beyond this he is also a close friend who spent several years with me in Cleveland where his brilliance, dry wit, and remarkable ability to cut through excreta won me over forever. Most of all, though, I owe Tom an unending debt of gratitude: you see, it was he who first introduced me to my wife, Yngvil. It just doesn't get better than that!

In closing I wish to commend the authors for their brilliant work and clear, practical writing, and the editors for their organizational talents and foresight. Finally, to you, the reader, I highly recommend this book. Drink deeply of it, read and reread the chapters, and you will come away with the practical knowledge you need to apply these important new techniques for the betterment of your patients.

James D. Thomas, MD, FACC, FAHA, FESC
Charles and Lorraine Moore Chair of
Cardiovascular Imaging
Department of Cardiovascular Medicine
Cleveland Clinic Foundation

Professor of Medicine and Biomedical
Engineering
The Ohio State University
and
Case Western Research University

Lead Scientist for Ultrasound
National Aeronautics and Space Administration

PART 1
Methodology

1

CHAPTER 1

Technical principles of tissue velocity and strain imaging methods

Andreas Heimdal

Introduction

Tissue velocity imaging (TVI) is an ultrasound technique that provides quantitative information on the velocity of the tissue. Traditionally, Doppler techniques have mainly been used to measure blood flow, and the signal component from tissue was considered noise that needed to be removed. There were early studies in the 1960s and 1970s using the pulsed-wave (PW) Doppler method to detect myocardial motion [1,2]. However, the method has had widespread use only since the late 1980s [3]. In the 1990s, color-coded TVI was introduced, allowing simultaneous velocity samples from an entire field of view [4–6]. This color TVI provides the possibility of extracting other parameters through spatial and temporal processing of the velocity data. Displacement, strain, and strain rate are examples of such parameters [7–9].

This chapter describes the technical aspects of TVI, including the acquisition technique, how the velocity is estimated, and how it may be presented and analyzed. The chapter also defines the parameters *displacement, strain,* and *strain rate* and explains how they can be derived from the tissue velocity data.

Tissue velocity imaging

TVI is a technique where the velocity of the myocardium toward or away from the transducer is measured and displayed. The velocities can be calculated and displayed as a PW spectrogram or as a color coding of the image. Both methods calculate the velocity based on the echoes of several ultrasound pulses fired in the same direction. The pulses are fired at a certain pulse repetition frequency (PRF). Each echo is sampled at a fixed depth, and the samples are collected into a new signal representing a certain position in the image. This signal is called the Doppler signal. The frequency of the Doppler signal is related to the velocity of the tissue in the sample region through the Doppler equation:

$$f_d = \frac{2f_0 v}{c}$$

In this equation, f_0 is the central frequency of the transmitted ultrasound pulse, c is the speed of sound, and v is the tissue velocity component in the ultrasound beam direction*.

Note that the Doppler equation also describes the frequency shift in a received pulse relative to the transmitted pulse. However, due to the short pulse length or, equivalently, the large bandwidth normally used for TVI, it is not feasible to estimate the frequency shift from one pulse only.

A consequence of using pulsed imaging is that there is a limit on the maximum velocity that can be measured. This limit is called the Nyquist velocity:

$$v_{\mathrm{Nyq}} = \frac{c \cdot \mathrm{PRF}}{4f_0}$$

If the actual velocity is higher than this limit, there will be frequency aliasing, resulting in misrepresentation of the velocity. The Nyquist velocity can be

*If second-harmonic Doppler imaging is used, the Doppler equations is $f_d = (4f_0 v)/c$.

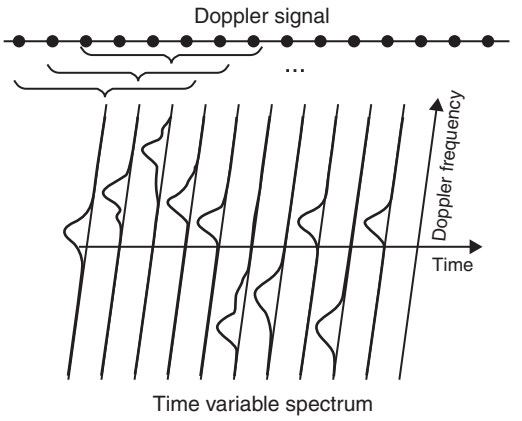

Figure 1.1 Generation of PW TVI. The Doppler signal is split into overlapping windows, and the frequency content of each window is calculated. Each circle in the illustration of the Doppler signal represents a sampled value.

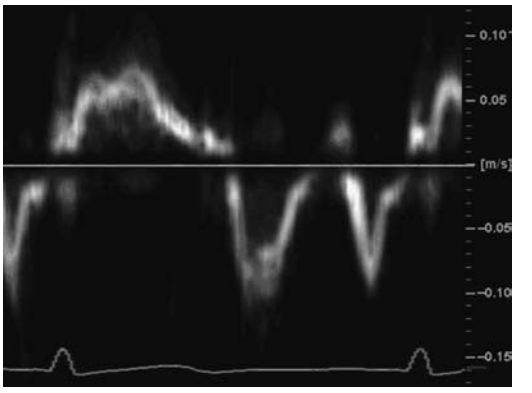

Figure 1.2 Example of PW TVI from the basal part of a healthy interventricular septum. The velocity variations over one full cardiac cycle are shown, as indicated by the electrocardiogram trace below the spectrum.

modified by adjusting the PRF or the ultrasound frequency f_0.

The combination of frequency, pulse length, and beam width that gives the optimal Doppler acquisition is not the same as that which gives good gray-scale image quality. Typically, lower frequencies, longer pulses, and wider beams are used for the Doppler acquisition. Therefore, the gray-scale image and the Doppler data are usually based on different acquisitions and may have different frame rates and spatial resolutions.

Pulsed-wave tissue velocity imaging

In PW TVI, the Doppler signal from only one sample region is collected. The signal is first split into overlapping windows, and then the frequency content of each window is calculated using the Fourier transform. Other, more advanced processing methods involving data from several sample regions may also be used. The result is a signal spectrum for each window, representing the frequency content at a certain time, as illustrated in Figure 1.1.

The spectral amplitude is next coded as gray-scale intensity, and the collection of signal spectra is visualized with Doppler frequency on the vertical axis and time on the horizontal axis. Because the Doppler frequency is linearly related to the tissue velocity, the vertical axis can also be a velocity axis. An example of PW TVI from the basal segment of a healthy interventricular septum is shown in Figure 1.2.

Note that the peak of each spectrum, representing the tissue velocity, is typically found in the *middle* of the spectral signal. The spectrum bandwidth, represented as the vertical thickness of the spectral signal, is related to the duration of the estimation windows. Using longer windows will typically give a smaller bandwidth, but at the same time, the temporal resolution will be reduced; therefore, there is a trade-off between accuracy and temporal resolution. Other factors that influence the bandwidth are acceleration in the tissue and acoustical noise.

Color tissue velocity imaging

In color TVI, a Doppler signal is collected for each depth and each ultrasound beam. This process normally requires more time, so each Doppler signal consists of fewer samples per time unit than in the PW case. This requirement normally limits the ability to calculate full-signal spectra for each position in the image. Instead, only the mean Doppler frequency is estimated for each position.

The most common way to estimate this mean frequency is to calculate the phase shift relative to the transmitted ultrasound pulse for each sample in the Doppler signal*. If the tissue is not moving, the phase shift is the same for all the samples. If the tissue is moving relative to the transducer, the phase shift increases or decreases from sample to sample according to the velocity of the tissue, as illustrated in Figure 1.3. The difference in phase shift from sample to sample in the Doppler signal can thus be

*A common way to calculate the phase shift is through the autocorrelation technique [10].

used to calculate the velocity. The sign of the phase corresponds to the sign of the estimated velocity.

When the velocity has been estimated for all parts of the ultrasound image, each pixel is color coded according to the velocity. As mentioned earlier, the Doppler acquisition is usually separate from the image acquisition; therefore, for each gray-scale image, there is at least one corresponding velocity image. The velocity image may have a lower resolution than the gray-scale image, but is normally interpolated to match the resolution of the gray-scale image. This finding means that neighboring pixels in the color-coded image may represent strongly correlated velocity values. The color code ranges from dark red for low velocities to bright yellow for high velocities toward the transducer, and from dark blue for low velocities to bright cyan for high velocities away from the transducer.

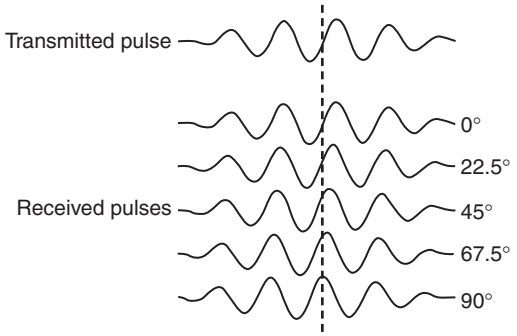

Figure 1.3 Illustration of echo pulses with increasing phase shifts relative to the transmitted pulse. A phase shift of 90° corresponds to half the Nyquist velocity.

Quantitative analysis

One of the major advantages of TVI is that it allows quantitative analysis of the motion pattern of the cardiac walls. In PW TVI, accurate timing and velocity measurements may be performed from the spectrogram. In color TVI, each pixel in the image represents a velocity measurement, and the quantitative value can be presented in various ways, as described in the following sections. The quantitative velocity values have been validated in vitro [11] and in vivo [12].

Time-traces

By picking one region of interest (ROI) in each frame of a color TVI cine-loop, the corresponding velocities can be presented as a time-trace, as illustrated in Figure 1.4. The time-trace represents the velocity pattern of the tissue within the ROI, similar to PW TVI. One of the differences between the two methods is that the PW TVI only can be acquired from one position at a time, whereas with color TVI, multiple time-traces from various regions can be generated from a single cine-loop. The PW TVI usually allows higher temporal resolution. The PW TVI in Figure 1.2 is taken from the same position and the same heart as the TVI time-trace in Figure 1.4.

The ROI used to generate the time-trace can be fixed to the same position in all the frames, or it can be moved to follow a certain anatomical structure.

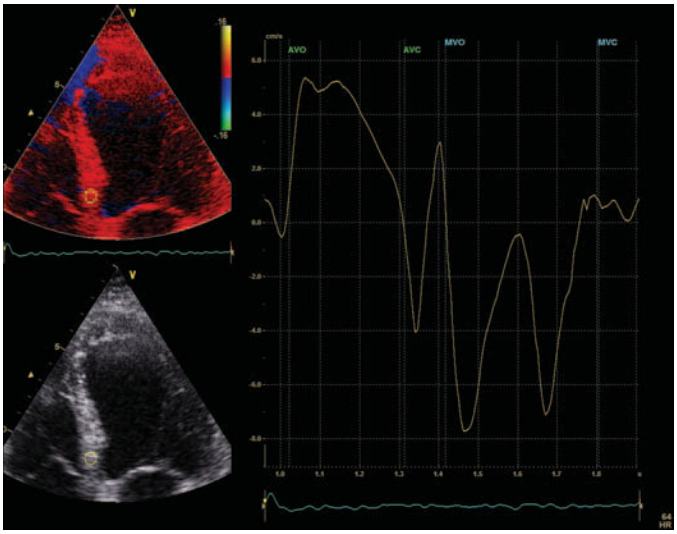

Figure 1.4 Example of a TVI time-trace from an ROI in the basal part of the interventricular septum of a healthy volunteer. The ROI is shown as a yellow circle in each of the left panels. An electrocardiogram trace is shown below the velocity trace. AVO, aortic valve opening; AVC, aortic valve closure; MVO, mitral valve opening; MVC, mitral valve closure.

To avoid having to adjust the position of the ROI in every single frame, it is recommended to reposition the ROI only in the extreme positions, and let the software perform a linear translation between these positions for the intervening frames. For a cardiac cycle, it is usually enough to anchor the ROI at three time instances: the onset of systole, the end of systole, and at the end of the early filling period.

Curved anatomical M-mode

Another way to visualize the color TVI data is to make an anatomical M-mode. The M-mode line may be a straight line in any direction through the two-dimensional (2-D) image. Alternatively, a curve may be manually drawn to an arbitrary shape, usually along the mid-myocardium. The resulting image is then called a curved anatomical M-mode (CAMM). Figure 1.5 shows an example of a TVI CAMM from the left ventricle of a healthy volunteer.

For apical views, the CAMM curve may be drawn separately in the two visible walls, or, as illustrated in Figure 1.5, the curve may be drawn from the base of one wall to the apex and down to the base of the other wall in one operation. The latter method produces a still CAMM image that represents the velocities of all the segments in all the 2-D frames.

Displacement imaging

When the velocity of the tissue is known, several other parameters can be derived. One of the simplest to calculate is displacement, which is the integral of the velocity over time:

$$d = \int_{T_0}^{T} v(t)\, dt$$

In this equation, T_0 and T are the start and end integration times, respectively, and $v(t)$ is the velocity at a given position at the time t. Typically T_0 is set to the beginning of systole and T to the end of systole to calculate the systolic displacement.

Displacement may be estimated from PW TVI recordings [13], but the calculation is more commonly based on color TVI data [7,14,15]. The method has been validated in vitro using a balloon phantom [11].

The displacement can be presented as a time-trace from an ROI, as a CAMM, or as a 2-D color-coded image. The latter is also known as a "Tissue Tracking" image, and an example is shown in Figure 1.6. A stepwise constant color coding, as opposed to a continuous color coding, is used for the Tissue Tracking image. With this method of color coding, it is possible to determine the strain, in addition to the displacement itself. Regions with narrow color bands have high strain, and regions with wide color bands have low strain. This concept will be described in more detail in the next section.

Figure 1.7 shows a velocity time-trace and the corresponding displacement time-trace from the basal part of the interventricular septum in a normal heart.

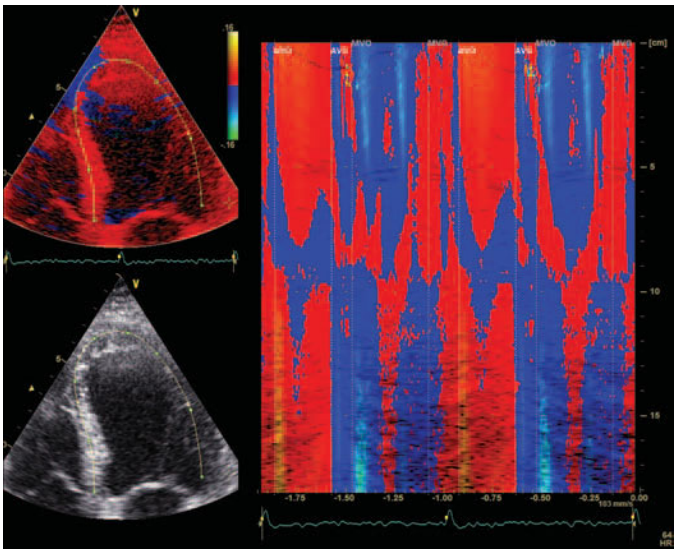

Figure 1.5 Example of a TVI CAMM over two cardiac cycles. The CAMM shows a map of the velocities at the locations indicated by the CAMM curve in the left panels. In this example, the upper, middle, and lower parts of the CAMM correspond to the septum, the apex, and the lateral wall, respectively. AVO, aortic valve opening; AVC, aortic valve closure; MVO, mitral valve opening; MVC, mitral valve closure.

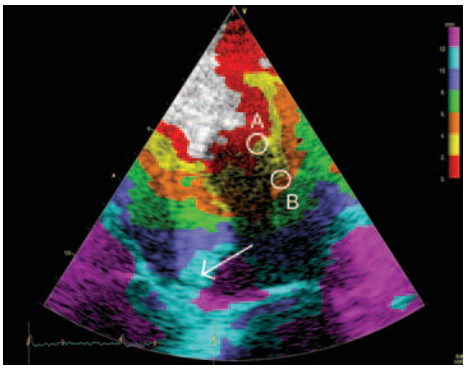

Figure 1.6 Example of a Tissue Tracking image of the heart of a normal volunteer, showing the end-systolic displacement. The start and end integration times are shown as red markers on the ECG trace. In this example, the basal part of the septum (arrow) is colored cyan, indicating a displacement of more than 10 mm. Similarly, the tissue in region A has moved 2 mm and the tissue in region B has moved 4 mm.

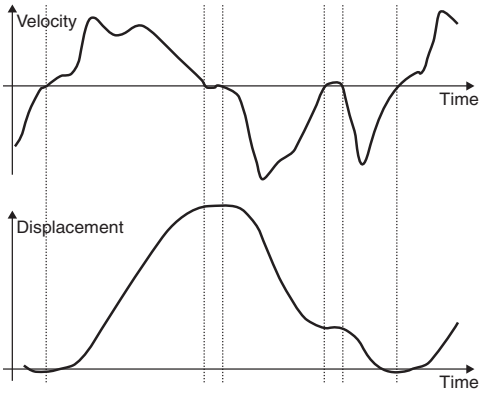

Figure 1.7 Comparison of velocity (top panel) and displacement (lower panel). The horizontal lines represent zero velocity or displacement, whereas the vertical dotted lines indicate when the velocity trace crosses zero.

As seen in these plots, the velocity is the slope of the displacement trace. When the velocity is positive, the displacement increases, and when the velocity is negative, the displacement decreases. When the velocity crosses zero, the displacement has a positive or negative peak, depending on the direction of the zero crossing.

When reporting displacement values, both the start and end integration times should be specified, for example: "The end-diastolic to end-systolic displacement was 10 mm." It is also important to specify in what direction the displacement was measured, that is, longitudinal or radial.

Concepts of strain and strain rate

Strain and strain rate are measures of changes in shape, that is, deformations. The use of these measures to describe mechanics of the heart muscle was introduced by Mirsky and Parmley in 1973 [16]. The strain and strain rate measures can be defined and estimated in various ways, as will be described in the following sections.

Definition of strain

Strain is a mechanical characteristic that describes the deformation of objects. There are several different ways to measure strain. For 1-D deformations, that is, shortening or lengthening, perhaps the simplest measurement is *conventional* or *engineering strain* $\varepsilon^{\star}$. It describes the relative change in length between two states. For an object of initial length L_0 that is being stretched or compressed to a new length L, the conventional strain is defined as:

$$\varepsilon = \frac{L - L_0}{L_0}$$

The Greek letter epsilon (ε) is commonly used as a symbol for conventional strain. The strain value is dimensionless and can be presented as a fractional number or as a percentage (by multiplying with 100). For instance, a fractional strain of −0.2 corresponds to a percentage strain of −20%. The strain is positive if L is larger than L_0, meaning that the object has lengthened, and negative if L is smaller than L_0, meaning that the object has shortened. If L equals L_0, there has been no change in length, and the strain is zero.

Other measures for 1-D strain include *natural strain*[†], which is defined as:

$$\varepsilon' = \ln\left(\frac{L}{L_0}\right)$$

*This strain measure has been named Lagrangian strain in the echocardiographic literature, but use of this term is not advised, because Lagrangian only means that the reference state is fixed, which is true for many strain measures. It is also known as longitudinal strain, but use of this term is not advised for cardiac applications, because it can be confused with the longitudinal direction of the ventricle.

[†]Natural strain is also termed logarithmic or true strain in the literature.

The name reflects the use of the natural logarithm function ln. Natural strain has the same properties as conventional strain regarding the sign: it is positive for lengthening, negative for shortening, and zero for no change in length. The actual strain, however, is slightly different for each method. Compared to that of conventional strain, the natural strain amplitude is smaller for positive strains and larger for negative strains. For instance, a conventional strain of 20% corresponds to a natural strain of 18.2%, and a conventional strain of −20% corresponds to a natural strain of −22.3%.

The conventional and natural strains have a fixed nonlinear relationship:

$$\varepsilon' = \ln(\varepsilon + 1)$$
$$\varepsilon = \exp(\varepsilon') - 1$$

Note that, in these formulas, the strains are represented as fractional numbers. For percentage strains, the corresponding formulas are:

$$\varepsilon'_{\%} = 100 \ln\left(\frac{\varepsilon_{\%}}{100} + 1\right)$$
$$\varepsilon_{\%} = 100\left(\exp\left(\frac{\varepsilon'_{\%}}{100}\right) - 1\right)$$

When reporting strain values, it should be specified whether conventional or natural strain is used. In addition, both the initial and the final reference states should be specified, for example: "The end-diastolic to end-systolic conventional strain was −20%." When measuring 1-D strains in a 2- or 3-D object, it is also important to specify in what direction the 1-D strains were measured.

Two- or three-dimensional strain

For 2- or 3-D deformations, the concept of strain becomes more complex. In the given coordinate system, one can use the 1-D strain in any spatial direction using the same definitions as presented earlier in this section. This type of strain is termed normal strain, because the deformation is normal to an imaginary plane. In addition, there might be shear strains, measuring changes in angle, as illustrated in Figure 1.8. The maximal and minimal strains might not occur in any of the coordinate directions; therefore, it is common to specify the directions and magnitudes of the maximal and minimal strains. These specifications are termed the principal strains and principal strain directions. Note that, if one aligns the coordinate system to the principal strain directions, there will be no shear strains.

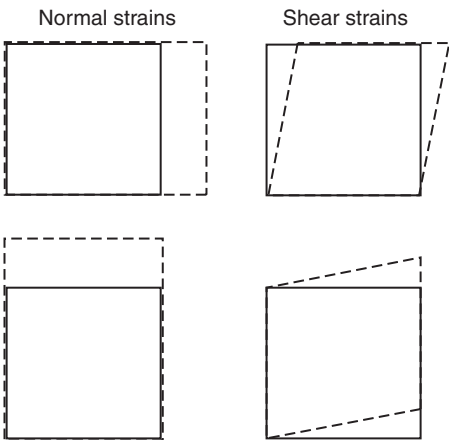

Figure 1.8 Illustration of normal strains (left) and shear strains (right).

Definition of strain rate

The strain rate is the temporal derivative of the strain:

$$\dot{\varepsilon} = \frac{d\varepsilon}{dt}$$

This definition means that, whereas strain indicates the amount of deformation, strain rate indicates the rate of the deformation. The relation between strain rate and strain can be compared to the relation between velocity and displacement. Assuming the velocity is constant, displacement equals time multiplied by velocity. Similarly, assuming the strain rate is constant, strain equals time multiplied by strain rate. A positive strain rate means that the length of the object is increasing, whereas a negative strain rate means that the length is decreasing. If the length is constant, the strain rate is zero.

The notation for strain rate is an epsilon with a dot above it ($\dot{\varepsilon}$), indicating the temporal derivative. Because this notation is cumbersome in many

instances, the acronym SR is commonly used to represent the strain rate. The unit of the strain rate is normally 1/sec or sec^{-1}, which may be read as "per second."* In other applications, the unit Hertz (Hz) is used for sec^{-1}, but this method is not recommended for strain rate. Hertz means number of oscillations per second, whereas for strain rate, it is more correct to speak of amount of deformation per second. A strain rate of -2 sec^{-1} applied over 1 sec would result in a relative strain of -2, and a corresponding percentage strain of -200%.

Note that, whereas the strain is a measurement of deformation relative to a reference state, the strain rate is an instantaneous measurement. There is no need to specify a reference state for strain rate, only the time of the measurement, for example: "The mid-systolic strain rate was -1.0 sec^{-1}."

Because there are several definitions of strain, there are a corresponding number of similar definitions for strain rate. In particular, the derivative of *natural strain* is†:

$$\dot{\varepsilon}' = \frac{d\varepsilon'}{dt} = \frac{1}{L}\frac{dL}{dt}$$

Estimation of strain and strain rate from ultrasound data

One way to measure strain is by M-mode through any of the cardiac walls [17,18]. By measuring the wall thickness before (L_0) and after (L) contraction, the transmural conventional strain can be calculated as:

$$\varepsilon = \frac{L - L_0}{L_0}$$

Another method is to use the displacement map provided by the Tissue Tracking modality. Consider the two regions marked A and B in Figure 1.6, and the distance between them L, which in this example is measured to 15 mm. Because region A is on the red–yellow color transition, it has moved 2 mm toward the transducer since the beginning of systole. Similarly, region B has moved 4 mm. This finding means that the length of the segment between A and B has been reduced by 2 mm. The original distance L_0 was thus 15 + 2 = 17 mm. By inserting these values into the equation for strain, one can calculate the strain to -12%. Generally, the closer together two color transitions are, the higher is the strain on the segment between them. A similar calculation may be performed based on PW TVI data [13].

Although accurate, these methods are relatively cumbersome to perform, especially for multiple cardiac segments. A faster method is to use TVI and calculate the strain rate and strain from the velocity data, as described in the following section.

Strain rate and velocity gradient

The spatial velocity gradient was one of the first parameters to be derived from TVI recordings [19–22]. With the assumption that the spatial velocity distribution within the estimation area is linear, the 1-D natural strain rate in an object is equivalent to the spatial velocity gradient [9]:

$$\dot{\varepsilon}' = \frac{dv}{dx}$$

This relation can be illustrated by considering the small object in Figure 1.9, which is being deformed. The instantaneous length is defined by the positions of the endpoints as $L = x_b - x_a$. Because the temporal derivative of spatial position

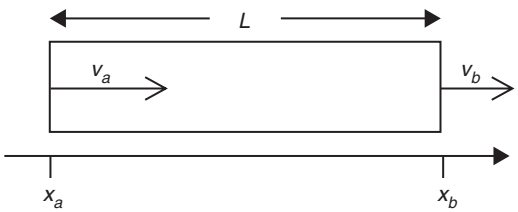

Figure 1.9 Illustration of a tissue segment of length L that is being deformed. The velocities of the endpoints x_a and x_b are v_a and v_b, respectively.

*In rare instances, the notation %/sec is seen for strain rate, meaning that the strain rate is multiplied by 100. A strain rate of -1 sec^{-1} corresponds to -100%/sec.

†The formula is derived using the relation $d(\ln(u))/dt = (du/dt)/u$.

is velocity, the natural strain rate of the object can be written as:

$$\dot{\varepsilon}' = \frac{1}{L}\frac{dL}{dt} = \frac{1}{L}\left(\frac{dx_b}{dt} - \frac{dx_a}{dt}\right) = \frac{v_b - v_a}{L} = \frac{dv}{dx}$$

Here, v_a and v_b are the instantaneous velocities of the endpoints of the segment.

In practice, it is rarely feasible to accurately track the endpoints of such a segment, and a fixed "strain length" Δx may be used instead. As long as the velocities are linearly increasing or decreasing within the region, this method will give exactly the same answer.

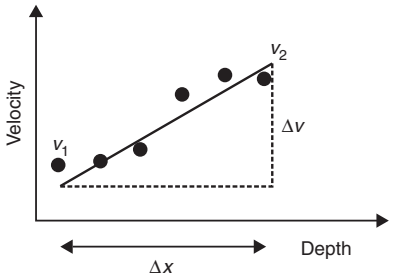

Figure 1.10 Illustration of the two methods to estimate strain rate from velocity data. The velocities v_1 and v_2 are the actual velocities of the endpoints, whereas Δv is the velocity difference of the endpoints of the regression line. See text for an explanation of the estimation methods.

As illustrated in Figure 1.10, the velocity gradient may be estimated using only the two velocity estimates v_1 and v_2 from the endpoints of the estimation area as:

$$\dot{\varepsilon}' = \frac{v_2 - v_1}{\Delta x}$$

or a linear regression of all the velocity samples within the area may be performed*:

$$\dot{\varepsilon}' = \frac{\Delta v}{\Delta x}$$

This method of measuring strain rate has been validated in vitro using tissue-mimicking phantoms [23,24] and in vivo versus wall motion scoring with standard echocardiography [25].

Note that the strain rate estimation is performed separately for each frame in a cine-loop and that the ROI may be moved from frame to frame to follow the motion of the myocardium, as explained earlier. Figure 1.11 shows an example of a color-coded strain rate image and an extracted strain rate trace.

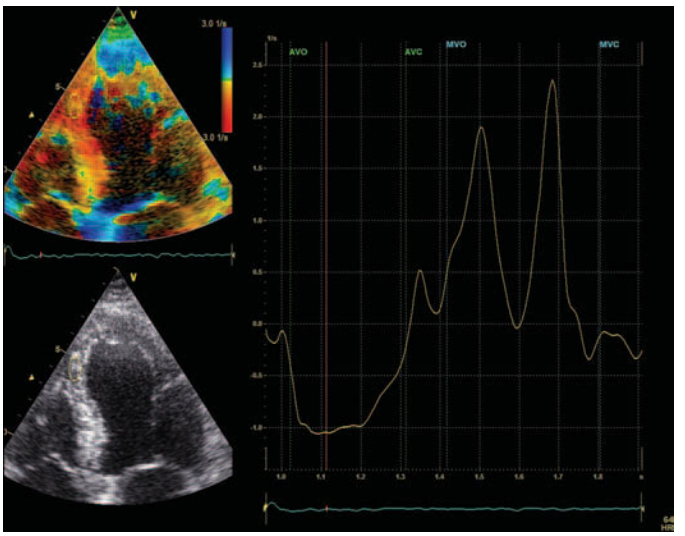

Figure 1.11 Mid-systolic strain rate images (left) and an extracted strain rate trace (right). The yellow ellipse in each strain rate image indicates the sample region for the trace. In healthy segments, the strain rate is typically negative in systole, indicating shortening, and positive in diastole, indicating lengthening. AVO, aortic valve opening; AVC, aortic valve closure; MVO, mitral valve opening; MVC, mitral valve closure.

*In ultrasound, velocities have been defined as positive for motion toward the transducer, whereas in the equations here, the velocities are defined as positive for increasing depth. This discrepancy may be accounted for by negating the velocity values before calculating the velocity gradient.

The color coding of strain rate typically ranges from yellow for low negative strain rates to red for high negative strain rates, and from light cyan for low positive strain rates to dark blue for high positive strain rates. A green color is sometimes used for the near zero strain rates.

Integrating strain rate to get strain

When the strain rate has been calculated for each time point during the deformation, the strain can be found as the temporal integral of the strain rate:

$$\varepsilon' = \int_{T_0}^{T} \dot{\varepsilon}'(t)\,dt$$

Here, T_0 and T are the time points of the start and end of the deformation. Note that it is the natural strain that is found through this integral. To find the more commonly used conventional strain, one might use the conversion formula:

$$\varepsilon = \exp(\varepsilon') - 1$$

Note also that, in commercially available post-processing tools, this function is normally performed automatically, so that it is the conventional strain that is presented to the user. The strain imaging method has been validated in vivo versus sonomicrometry [26] and tagged magnetic resonance imaging [27]. The color coding for strain is typically red for negative strain and blue for positive strain, as illustrated in Figure 1.12.

Artifacts and methods to improve signal quality

As are all ultrasound modalities, tissue velocity and strain imaging are also affected by noise components such as random thermal noise and reverberations. These noise components may degrade the quality of the velocity and strain rate measurements. In addition, angle mismatches between the ultrasound beams and the examined structure may cause errors. The artifacts, and suggestions of how to reduce them, are reviewed in the following sections.

Reverberation artifacts

Reverberations are false echoes resulting from multiple reflections within the body. In the gray-scale image they are seen as false echoes or reduced contrast. The reverberations are often caused by tissue layers close to the body surface. These layers are relatively motionless, and the reverberation artifacts are, therefore, often seen as immobile structures mixed with the true signal.

In PW TVI, reverberations can be seen as an increased intensity at zero velocity, as shown in Figure 1.13. In many cases, it is still relatively easy to identify the true velocity signal. PW TVI may,

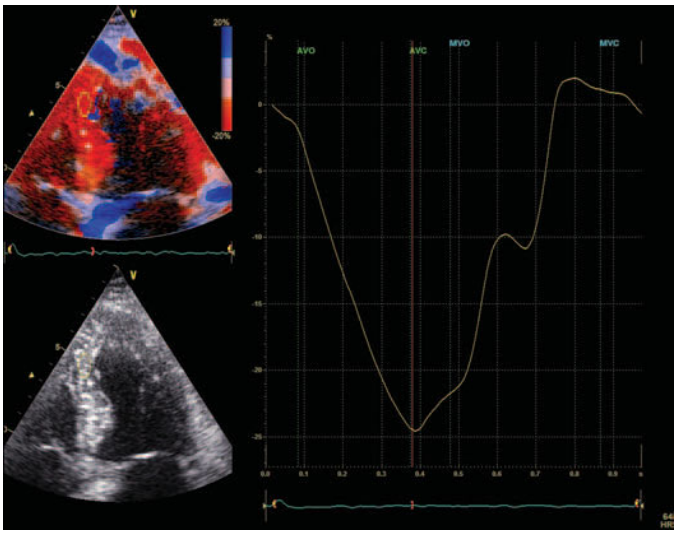

Figure 1.12 End-systolic strain images (left) and an extracted strain rate trace (right). The yellow ellipse in each strain rate image indicates the sample region for the trace. In healthy segments, the strain is typically negative at end-systole, indicating shortening, and returns to zero at end-diastole. AVO, aortic valve opening; AVC, aortic valve closure; MVO, mitral valve opening; MVC, mitral valve closure.

therefore, be a preferred method for velocity measurements in patients with poor acoustic windows.

For color TVI, strong reverberations may cause a bias in the mean velocity estimate, as shown by the trace in Figure 1.13. Typically the bias is toward zero velocity. The amount of bias depends on the intensity of the reverberation signal relative to the tissue velocity signal. However, the sign of the velocity is seldom affected, so it might be difficult to detect reverberations from the TVI color display, as illustrated in the central part of Figure 1.14.

In strain rate imaging, reverberations may cause large errors, as illustrated in Figure 1.14. A small local bias in the velocity will cause large changes in the spatial velocity gradient and, thus, the strain rate. A typical reverberation artifact in strain rate is a strong blue and red stripe next to each other. Figure 1.15 shows an example of how a strain rate artifact may be detected by using CAMM.

Displacement and strain are calculated from velocity and strain rate; therefore, reverberation errors in velocity and strain rate will also cause errors in displacement and strain. Because strain rate is most affected by reverberation errors, strain will be more affected than displacement.

Unfortunately, there is little the user can do when there is reverberation noise, other than trying to get the best scanning window when performing the imaging. When analyzing the strain rate data, it is important to recognize the reverberation artifacts and to avoid the regions affected. CAMM may, as illustrated in Figure 1.15, be a good tool to get an overview of the amount of reverberation artifacts in the strain rate and may be used prior to detailed analysis.

Angle dependence

All basic Doppler methods are angle dependent. It is only the velocity component in the ultrasound beam direction that is picked up. If the true velocity direction is known – or assumed – the true velocity may be calculated by dividing the measured velocity component by $\cos(\theta)$, where θ is the angle between the ultrasound beam and the true velocity direction [20]. This explanation means that, as the angle increases, the measured velocity component decreases from 100% of the true velocity at zero angle to 0% at a 90°, as illustrated in Figure 1.16.

For strain rate, the angle dependence is more complex. Assuming, for simplicity, that the beam

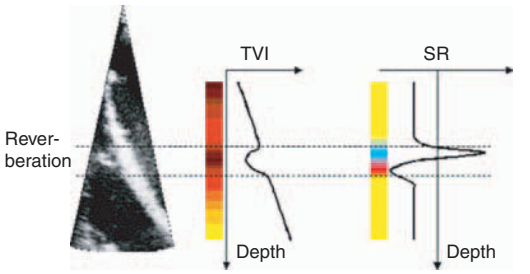

Figure 1.14 Illustration of effect of a local reverberation in the mid-septum on the tissue velocity and strain rate (SR). The color bars indicate the coloring of the septum in mid-systole, whereas the plots show the actual velocities and strain rates at different depths along the septum. The dashed lines indicate the region affected by the reverberation.

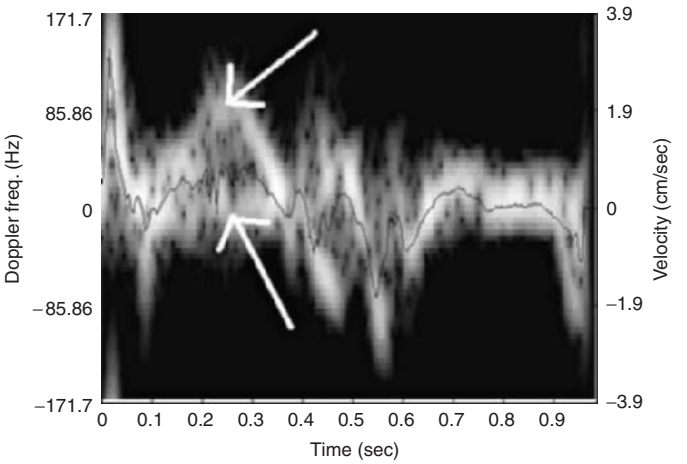

Figure 1.13 PW TVI from a region with strong reverberations. The upper arrow shows the true signal, and the lower arrow shows the reverberation artifact centered around zero Doppler frequency. The black trace shows the corresponding TVI trace based on color TVI. As one can see, the TVI trace underestimates the correct velocity value.

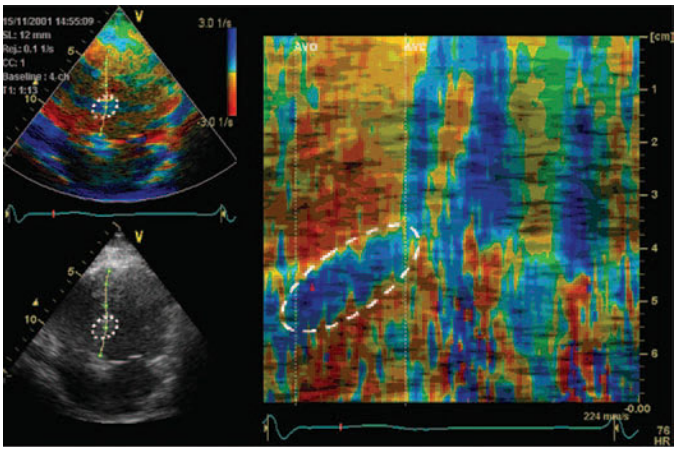

Figure 1.15 Strain rate image (top left) and a derived CAMM image (right) showing an artifact region covering the basal part of the interventricular septum (white ellipses). Artifacts can often more easily be detected in the CAMM display than in the 2-D strain rate image. AVO, aortic valve opening; AVC, aortic valve closure; MVO, mitral valve opening; MVC, mitral valve closure.

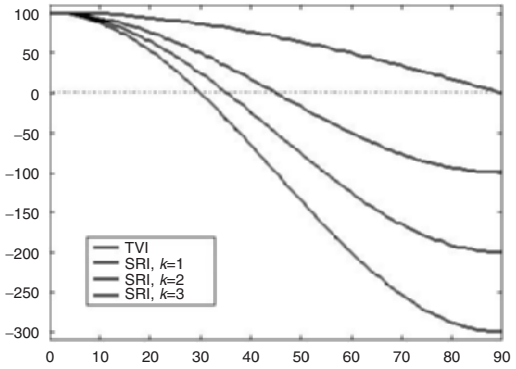

Figure 1.16 Angle dependence of TVI and strain rate imaging (SRI) for three different assumptions of the radial–longitudinal relationship (k). The graphs show how many percent of the true value is picked up when the angle between the ultrasound beam and the desired direction increases. For TVI, it is assumed that the true velocity is in the direction of the ultrasound beam. Notice that, whereas the measured velocity component drops to 0% at 90°, the strain rate becomes zero at 45° or lower.

is perpendicular to the circumferential direction, which usually is the case for apical imaging, a relation can be formulated. Assuming also no shear, the measured strain rate is a component of both the longitudinal (l) and the radial (r) strain rates [28]:

$$\dot{\varepsilon} = \dot{\varepsilon}_l \cos^2\theta + \dot{\varepsilon}_r \sin^2\theta$$

Figure 1.16 shows the angle dependence of the measured strain rate as the percentage of the longitudinal strain rate for various values of the assumed linear relation:

$$k = -\frac{\dot{\varepsilon}_r}{\dot{\varepsilon}_l}$$

Since the value of k is generally unknown, it is not possible to angle-correct the measured strain rate. Also, the assumptions of no shear and linear relation between radial and longitudinal strain rates are in general not fulfilled; therefore, the model is somewhat inaccurate. However, the model may give some indications of the angle dependence of the estimate.

Note that strain rate is more angle dependent than tissue velocity. For example, assuming $k = 3$, the measured strain rate is reduced to 50% of the true value at 20°, whereas the measured tissue velocity is still 94% of the true value at the same angle. It is, therefore, important to align the ultrasound beams with the muscle when measuring longitudinal strain rates and strains. To be able to accomplish this alignment, it might be necessary to image the different walls and segments of the heart with different probe positions.

Uematsu et al. [20] have suggested using angle-corrected velocities as a basis for the strain rate estimation. The method relies on user input to define the true direction of the motion. With this method, the strain and strain rate in any spatial direction may be calculated, except in the regions where the assumed motion directions are perpendicular to the ultrasound beams. In these regions, it is not possible to angle-correct the velocities.

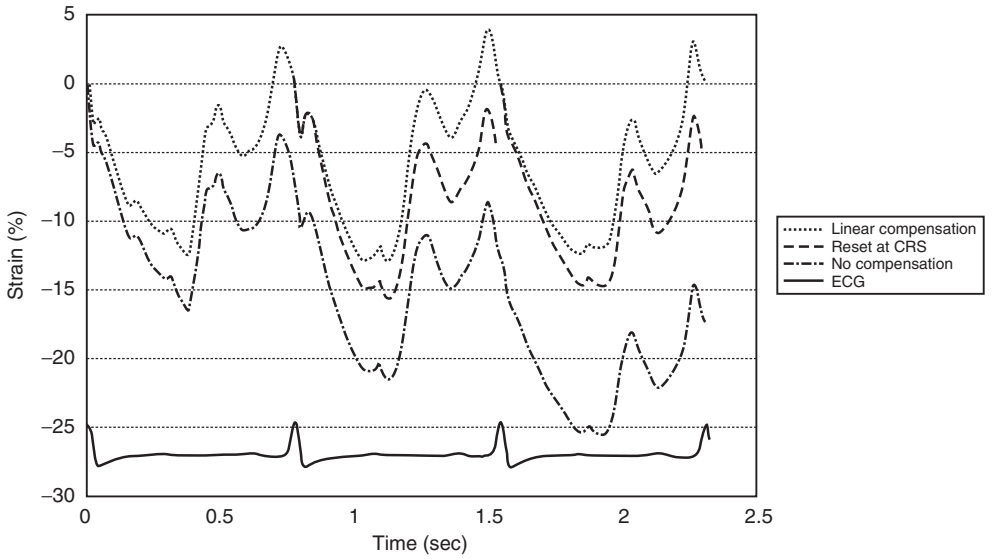

Figure 1.17 Drift compensation of a strain trace. The dash-dotted trace is the original uncompensated strain trace, while the dashed and dotted traces are drift compensated. The dashed trace is reset at every QRS but does not necessarily return to zero at the end of each heart beat. The dotted brace is forced to end at zero at each beat through linear compensation. ECG, electrocardiogram trace.

Drift and drift compensation

Ideally, for displacement and strain traces, the curve should return to the same value, normally zero, at the start of each heartbeat. Artifacts such as those mentioned earlier may result in a drift from beat to beat, meaning that the curve does not return to the same value.

This drift may be compensated in two ways: by forcing the curve to start at the same value in every heartbeat, or through linear compensation of the values in all the time points. Figure 1.17 shows examples of the two methods on a strain trace. Note that the peak strain value is changed when using linear compensation. For the reset-at-zero method, the difference between start and end within a heartbeat is not changed. For example, in the second heartbeat in Figure 1.17, the peak strain in the trace reset at QRS is −16%. By subtracting the starting value for the uncompensated trace (−6%) from the peak value (−22%), the exact same peak strain of −16% is found.

Noise reduction by averaging

Spatial and temporal averaging may be helpful to reduce random noise. Note that reverberation artifacts and errors caused by angle mismatch are generally not of random nature, so averaging will generally not improve these artifacts.

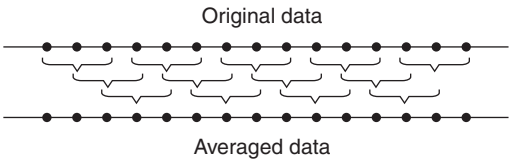

Figure 1.18 Illustration of the "sliding window" technique that can be used in the averaging process. The averaged data may have the same sample resolution as the original data, but neighboring samples will be correlated.

All averaging techniques may be performed using a "sliding window" technique as illustrated in Figure 1.18. Every sample in the averaged data is based on a set of samples in the original data. The set can be a collection of spatial and/or temporal samples. Spatial averaging is usually performed along the ultrasound beams (axial averaging), perpendicular to them (lateral averaging), or a combination of the two. Temporal averaging may be performed by combining data from a set of frames.

Note that the sample resolution in the averaged data is the same as in the original data, but that

neighboring samples in the averaged data will be correlated. This finding means that averaging should not be performed in the directions where the user wants to measure differences. For example, if the user wants to study differences between subendocardial and subepicardial longitudinal strain rate, no averaging should be performed between the beams in apical views.

A special form of temporal averaging can be performed by averaging only samples from the same time after QRS in several heartbeats. This type of averaging is termed *cine-compound*.

References

1 Yoshida T, Mori M, Nimura Y, et al. Analysis of heart motion with ultrasonic Doppler methods and its clinical applications. *Am Heart J* 1961; **61:** 61–75.

2 Kostis JB, Mavrogeorgis E, Slater A, Bellet S. Use of a range-gated, pulsed ultrasonic Doppler technique for continuous measurement of velocity of the posterior heart wall. *Chest* 1972; **62:** 597–604.

3 Isaaz K, Thompson A, Ethevenot G, Cloez JL, Brembilla B, Pernot C. Doppler echocardiographic measurement of low velocity motion of the left ventricular posterior wall. *Am J Cardiol* 1989; **64:** 66–75.

4 McDicken WM, Sutherland GR, Moran CM, Gordon LN. Colour Doppler velocity imaging of the myocardium. *Ultrasound Med Biol* 1992; **18:** 651–4.

5 Sutherland GR, Stewart MJ, Groundstroem KW, et al. Color Doppler myocardial imaging: a new technique for the assessment of myocardial function. *J Am Soc Echocardiogr* 1994; **7:** 441–58.

6 Yamazaki N, Mine Y, Sano A, et al. Analysis of ventricular wall motion using color-coded tissue Doppler imaging system. *Jpn J Appl Phys* 1994; **33:** 3141–6.

7 Pan C, Hoffmann R, Kuhl H, Severin E, Franke A, Hanrath P. Tissue tracking allows rapid and accurate visual evaluation of left ventricular function. *Eur J Echocardiogr* 2001; **2:** 197–202.

8 Heimdal A, Stoylen A, Torp H, Skjaerpe T. Real-time strain rate imaging of the left ventricle by ultrasound. *J Am Soc Echocardiogr* 1998; **11:** 1013–9.

9 D'hooge J, Heimdal A, Jamal F, et al. Regional strain and strain rate measurements by cardiac ultrasound: principles, implementation and limitations. *Eur J Echocardiogr* 2000; **1:** 154–70.

10 Kasai C, Namekawa K, Koyano A, Omoto R. Real-time two-dimensional blood flow imaging using an autocorrelation technique. *IEEE Trans Sonics Ultrason* 1985; **32:** 458–64.

11 Wu Y, Irvine T, Mori Y, Li X, Sahn DJ. In vitro validation of tissue Doppler left ventricular regional wall velocities by using a novel balloon phantom. *J Tongji Med Univ* 2001; **21:** 337–40.

12 Donovan CL, Armstrong WF, Bach DS. Quantitative Doppler tissue imaging of the left ventricular myocardium: validation in normal subjects. *Am Heart J* 1995; **130:** 100–4.

13 Hartley CJ, Latson LA, Michael LH, Seidel CL, Lewis RM, Entman ML. Doppler measurement of myocardial thickening with a single epicardial transducer. *Am J Physiol* 1983; **245:** H1066–72.

14 Cain P, Khoury V, Short L, Marwick TH. Usefulness of quantitative echocardiographic techniques to predict recovery of regional and global left ventricular function after acute myocardial infarction. *Am J Cardiol* 2003; **91:** 391–6.

15 Cain P, Baglin T, Khoury V, Case C, Marwick TH. Automated regional myocardial displacement for facilitating the interpretation of dobutamine echocardiography. *Am J Cardiol* 2002; **89:** 1347–53.

16 Mirsky I, Parmley WW. Assessment of passive elastic stiffness for isolated heart muscle and the intact heart. *Circ Res* 1973; **33:** 233–43.

17 Guth B, Savage R, White F, Hagan A, Samtoy L, Bloor C. Detection of ischemic wall dysfunction: comparison between M-mode echocardiography and sonomicrometry. *Am Heart J* 1984; **107:** 449–57.

18 Shapiro E, Marier DL, St John Sutton MG, Gibson DG. Regional nonuniformity of wall dynamics in normal ventricle. *Br Heart J* 1981; **45:** 264–70.

19 Fleming D, Xia X, McDicken WN, Sutherland GR, Fenn L. Myocardial velocity gradients detected by Doppler imaging. *Br J Radiol* 1994; **67:** 679–88.

20 Uematsu M, Miyatake K, Tanaka N, et al. Myocardial velocity gradient as a new indicator of regional left ventricular contraction: detection by a two-dimensional tissue Doppler imaging technique. *J Am Coll Cardiol* 1995; **26:** 217–23.

21 Palka P, Lange A, Fleming AD, et al. Differences in myocardial velocity gradient measured throughout the cardiac cycle in patients with hypertrophic cardiomyopathy, athletes and patients with left ventricular hypertrophy due to hypertension. *J Am Coll Cardiol* 1997; **30:** 760–8.

22 Derumeaux G, Ovize M, Loufoua J, Pontier G, Andre-Fouet X, Cribier A. Assessment of nonuniformity of transmural myocardial velocities by color-coded issue Doppler imaging. *Circulation* 2000; **101:** 1390–5.

23 Belohlavek M, Bartleson VB, Zobitz ME. Real-time strain rate imaging: validation of peak compression and expansion rates by a tissue-mimicking phantom. *Echocardiography* 2001; **18:** 565–71.

24 Hashimoto I, Mori Y, Rusk RA, et al. Strain rate imaging: an in vitro "Validation" study using a physiologic balloon model mimicking the left ventricle. *Echocardiography* 2002; **19:** 669–77.

25 Stoylen A, Heimdal A, Bjornstad K, Torp HG, Skjaerpe T. Strain rate imaging by ultrasound in the diagnosis of regional dysfunction of the left ventricle. *Echocardiography* 1999; **16:** 321–9.

26 Urheim S, Edvardsen T, Torp H, Angelsen B, Smiseth OA. Myocardial strain by Doppler echocardiography. Validation of a new method to quantify regional myocardial function. *Circulation* 2000; **102:** 1158–64.

27 Edvardsen T, Gerber BL, Garot J, Bluemke DA, Lima JA, Smiseth OA. Quantitative assessment of intrinsic regional myocardial deformation by Doppler strain rate echocardiography in humans: validation against three-dimensional tagged magnetic resonance imaging. *Circulation* 2002; **106:** 50–6.

28 Heimdal A. *Doppler based ultrasound imaging method for noninvasive assessment of tissue viability* [Doktor ingeniør thesis]. Trondheim: Norwegian University of Science and Technology; 1999.